JOURNAL OF GEOPHYSICAL RESEARCH, VOL. 103, NO. C11, PAGES 24,969–24,982, OCTOBER 15, 1998

COASTWATCH'95: ERS 1/2 SAR detection of natural film on the ocean surface

H. A. Espedal,[1] O. M. Johannessen,[1,2] J. A. Johannessen,[3] E. Dano,[4]
D. R. Lyzenga,[5] and J. C. Knulst[6]

Abstract. Ocean mesoscale phenomena such as eddies and current convergence zones can often be seen in synthetic aperture radar (SAR) images due to characteristic patterns caused by natural film induced damping of the waves. Such films have also been found to exert a significant effect on air–sea gas exchange, which may be important for the global scale climate system. Satellite SAR may prove very useful to quantify the extent of natural film. To investigate the composition of these films and their effect on radar return, we compared samples of the sea surface with ERS 1/2 SAR images of coastal ocean areas during the COASTWATCH'95 experiment. Simultaneous observations were made with a shipmounted C band dual–polarized Doppler radar, and surface drifters were deployed to investigate the surface current variations in the vicinity of different slicks (areas where the short surface waves sensed by a radar are damped). One confirmed case of natural film was thus verified to be caused by a convergence zone. The study also showed that the films investigated during COASTWATCH'95 were generally less concentrated and originated from marine organisms, compared to the films with terrestrial influences found in a previous experiment in a fjord [*Espedal et al.*, 1996]. The dependence of the existence of the films on wind speed is also investigated, and an estimate of natural film distribution during the experiment period is given, using a total of 71 ERS 1/2 SAR images collected over the same coastal area under a variety of wind conditions. Up to 40% natural film coverage was found for 2.5 m/s wind speeds, while already at 5–10 m/s all SAR imagery had under 5% film coverage.

1. Introduction

Natural film on the ocean surface is formed from marine organisms or terrestrial material delivered by runoff or atmospheric transport. The composition of natural films varies, but substances such as proteins, lipids, saccharides, organic acids, and metals associated with the organic matter are usually present at higher concentrations than those in the corresponding bulk water [*Duce et al.*, 1994; *Espedal et al.*, 1996]. Film material accumulates in regions of high biological activity, i.e., in coastal regions, in the marginal ice zone, in regions of upwelling, along converging current boundaries, and in eddies. Sea surface films have been seen to influence energy dissipation in capillary waves [*Lucassen-Reynders and Lucassen*, 1969; *Hühnerfuss et al.*, 1987], gas exchange rates [*Frew et al.*, 1990], and marine aerosol formation [*Gershey*, 1983]. *Asher* [1997] has estimated that the impact of various hypothetical slick coverages on global air–sea CO_2 exchange is important. However, global spatial film quantification has not yet been done, and it is therefore difficult to know whether natural films really are extensive enough to be of importance in global change studies.

The spaceborne synthetic aperture radar (SAR), with its high spatial resolution (25m), may contribute significantly in global mapping of natural films on the ocean surface during moderate wind conditions, when film can be detected. Damping of the capillary and short gravity waves by the film, sensed by radars via Bragg backscatter, produce dark slick signatures in the SAR imagery. So far, oil slicks have been investigated and are well documented in satellite SAR images [*Wismann*, 1993; *Espedal et al.*, 1995; *Wahl et al.*, 1996]. Moreover, artificial monomolecular films have been studied a number of times with airborne radars [*Alpers et al.*, 1991; *Hühnerfuss et al.*, 1994]. In contrast, only one previous study exists in which the chemical components of

[1]Nansen Environmental and Remote Sensing Center, Bergen, Norway.
[2]Also at Geophysical Institute, University of Bergen, Norway.
[3]European Space Research and Technology Centre, Noordwijk, The Netherlands.
[4]Department of Naval Architecture and Marine Engineering, University of Michigan, Ann Arbor.
[5]Environmental Research Institute of Michigan, Ann Arbor.
[6]Swedish Environmental Research Institute, Aneboda, Sweden.

Paper number 98JC01660.
0148-0227/98/98JC-01660$09.00

natural films were sampled simultaneously with satellite SAR acquisition. This experiment was conducted under calm wind conditions in a Norwegian fjord [*Espedal et al.*, 1996] and showed that there exists a chemical difference between slicked and nonslicked areas in the ERS 1 SAR image. The concentration of fatty acids was generally 1 order of magnitude higher inside than outside natural film areas, and a corresponding 6–17 dB decrease in SAR backscatter was found.

The primary objective of the work reported here was to extend the documentation of the composition of natural films and their effect on radar return to include different coastal and atmospheric conditions. This work may in turn give new valuable insight into the processes responsible for accumulation of different natural films in coastal areas. Eventually, this may also help to develop satellite SAR as a tool in mapping the global extent, distribution, and variability of natural films, to be used, for example, in global change studies. From a practical point of view, knowledge of natural films is perhaps more important for SAR oil spill detection systems, since these films are difficult to distinguish from oil in the SAR imagery [*Espedal,* 1998].

During the COASTWATCH'95 experiment, samples of the sea surface microlayer and subsurface water were taken simultaneously with C band Doppler radar measurements and ERS SAR coverage of the ocean surrounding the southwest coast of Norway [*Johannessen et al.,* 1996]. The experiment is described in section 2, and three special slick cases are discussed in section 3. Estimates of natural film distribution, based on 71 ERS SAR images from the experimental region, are also given. In section 4 a general discussion of the results shows that increased concentrations of free fatty acids inside slicks corresponded with damping in the Doppler radar data and the ERS SAR imagery. A comparison is made with data from the earlier natural film–SAR experiment in Korsfjord [*Espedal et al.,* 1996], indicating that the fatty acids found during COASTWATCH'95 originate from marine organisms, in contrast to the terrestrial sources found for the Korsfjord samples. Furthermore, the damping was lower, 2-11 dB during COASTWATCH'95 in comparison with 6-17 dB in Korsfjord SAR imagery. In section 5 we draw conclusions that emphasize the importance of a properly developed natural film discrimination algorithm based on satellite SAR.

2. The COASTWATCH'95 Experiment

A tandem ERS 1/2 experiment was carried out off the southwestern coast of Norway (Figure 1) during the month of September 1995 [*Johannessen et al.,* 1996]. The main objectives of this experiment were to investigate and quantify natural films, coastal jets, ocean fronts, wind velocity, wind fronts, and rain showers from ERS 1/2 SAR. Information from the C band (5.3 GHz) vertical transmit and receive (VV) polarized SAR images in near real time were used to navigate the research vessel R/V *Håkon Mosby* to different SAR features of interest. A unique integrated data set was collected, including extensive SAR coverage in the ERS 1/2 tandem mode, ATSR and NOAA advanced very high resolution radiometer (AVHRR) data, an extensive set of oceanographic and meteorological variables from the R/V *Håkon Mosby* (e.g., wind, air temperature at ~10 m above sea surface, and sea temperature at 4 m depth), ship-mounted dual-polarized Doppler radar observations, metocean parameters from a state-of-the-art metocean buoy, and natural slick sampling with two radio-controlled "mini research vessels."

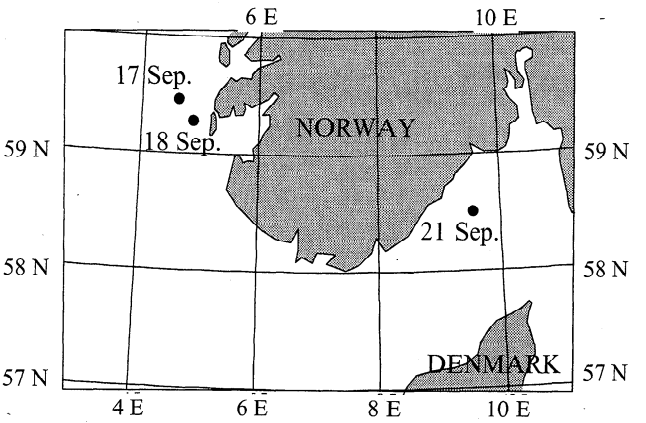

Figure 1. The experimental area, showing the location of the three slick studies discussed in section 3. During the field cruise period from September 11 to October 1, 1995, the SAR coverage of the ocean area shown on the map was almost complete (except east of 10°E).

2.1. Remote Sensing

Extensive temporal and complete spatial satellite SAR coverage of the experiment region (Figure 1) was possible because the ERS 1/2 tandem mission provided exact repeat coverage on ground with 24–hour separation. There were also crossovers from ascending/descending ERS passes at ~11 to 13–hour separation. A total of 53 SAR scenes (each covering 100 × 100 km) from the experiment region were analyzed during the field campaign from September 11 to October 1, 1995. In addition, 18 scenes covering the same region before (August–September) and after (October) the experiment have been analyzed in this work. Both full-resolution (25 m) and low-resolution (100 m) ERS SAR images (23° incidence angle) have been used.

2.2. C band Doppler Radar

A C band (4.92 GHz) continuous wave (CW) Doppler scatterometer with VV and HH polarization (Figure 2) was installed to acquire shipborne radar backscatter measurements during COASTWATCH'95 [*Dano and Kletzli,* 1996]. Similar CW radars have been successfully used in several other laboratory and open ocean experiments [*Keller and Plant,* 1990; *Jessup et al.,* 1991; *Hara et al.,* 1994; *Lee et al.,* 1995; *Walker et al.,* 1996]. The Doppler scatterometer measures the backscattered power (radar cross section, or RCS) from which surface roughness is calculated. The surface current is retrieved

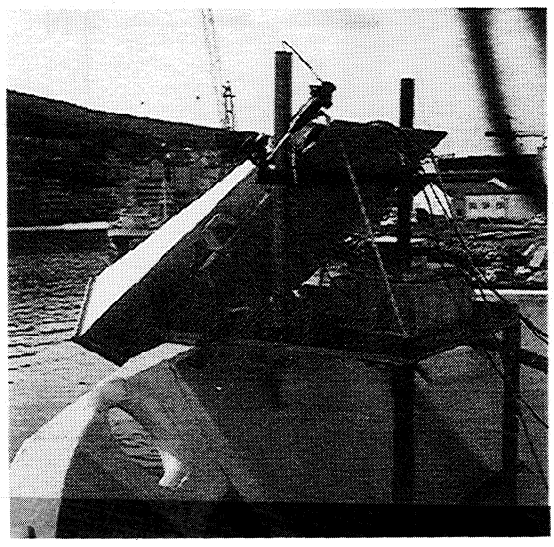

Figure 2. Photograph of the C band Doppler scatterometer.

from the Doppler shift (spectral mean), and hence surface current gradients can be measured at very fine spatial resolution (approximately meters). In addition, the spectral width provides a measure of the distribution of the speeds of scatterers. If just a single scatterer existed, moving at a fixed (constant) speed, then theoretically, the spectral width would be zero. On the ocean, however, the scatterers are being tilted and advected by wind waves, and the Doppler width can be expected to be broad. When the return is close to the noise floor (i.e., in a slick), the Doppler width will artificially broaden, since white noise theoretically has an infinite bandwidth. Therefore no currents can be retrieved from the Doppler data in regions affected by such system noise.

The scatterometer was mounted on the bow of the R/V *Håkon Mosby*, 6.5 m above the water level at an angle of 45° (in relation to the ship's vertical axis). The two-way half-power beam width was 9° for both the horizontally and vertically polarized radiation. This yielded a half-power footprint ("spatial resolution") of approximately 2 m in the along-track direction and 1.5 m in the cross-track direction on the water surface. Measurements were typically made with the ship moving at a speed of 2–3 m/s. The RCS and spectral statistics plots in this work are generally based upon a 35 s running average equal to a distance of ~100 m, for more easy comparison with low-resolution SAR imagery (100 m). However, this will tend to smear out the apparent width of the actual transition regions. Furthermore, only VV polarization results are discussed in this paper, enabling a more direct comparison with the VV-polarized ERS SAR. Details of the construction of the radar and calculations of spectral mean and currents are described in the appendix.

2.3. Slick Sampler

During the first part of the COASTWATCH'95 experiment (September 11–19), surface microlayer material was collected by using two remotely controlled samplers, INTERFACE I (length 1.2 m) and II (length 2 m) [*Knulst*, 1996]. Both were equipped with a rotating hydrophilic Teflon drum [*Harvey*, 1966]. *Knulst* [1996] discusses some of the properties of the Teflon drum used in surface microlayer sampling. Laboratory studies show that some degree of specific adsorption occurs and that no leakage of heavy metals or organic substances occurs from the drum Teflon (for fatty acids (FA) and alkanes (ALK) studied here there is a 2.0 μg/l detection threshold). The INTERFACE II (Figure 3) was also fitted with a Global Positioning System (GPS) receiver, temperature probes, an anemometer, and a data logger. Bulk water samples were obtained at 20 cm depth for comparison. The samples were analyzed for salinity, anions (NO_2–N, NH_4–N, Cl, and SO_4–S), fatty acids (even-numbered C12–C18), alcanes (total aliphatic hydrocarbons C18–C32), total organic carbon (TOC), cations (Na, K, Ca, Mg), and trace metals (Fe, Mn, Al, As, Ba, Cd, Co, Cr, Cu, Hg, Ni, Pb, and Zn). Ultraviolet (UV) and visual light (VIS) scans were made on all samples, and pH, specific conductivity, and turbidity were determined.

Wind speed on INTERFACE II was measured at +100 cm with SENTRY model 03105 cup anemometer (R.M. Young Electronics, Traverse City, Michigan). Air temperature was measured at +80 cm with a 107 temperature probe (Campbell Scientific Ltd., Sheepshead, United Kingdom) fitted with a 10TCRT thermocouple reference probe and covered with Youngs gill multiplate radiation shield. Water temperatures were measured at 0 to -0.3 cm for microlayer and -20 cm for bulk, with silver–copper thermocouples (0.17 mm wire gauge). Measurements made 180 times per minute were averaged as 1 min mean values and logged on a CR10 Campbell logger. Salinity was calculated from a combination of chloride (determined titriometrically) and specific conductivity of the sample. The sensitivity is ±0.5‰. Alkanes and fatty acids analyses were performed on microcapillary gas chromatograph with a flame ionization detector (GC–FID). Before analysis, standard substances (25 μg dibromodecanoic acid and 25 μg alpha–cholestane) were added to the 100–500 mL samples, and the organic phase was extracted with solvents. The solvent extract was concentrated to

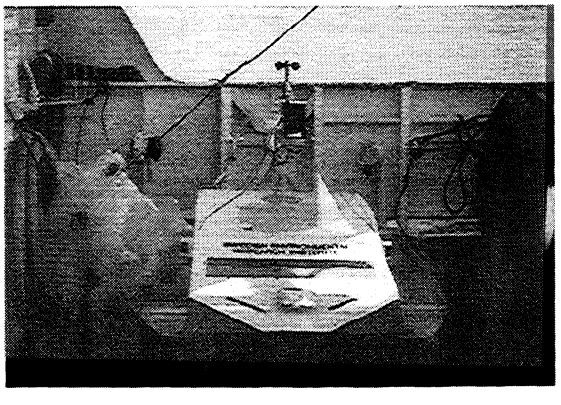

Figure 3. The sea surface slick sampler Interface II.

near dryness, and the fatty acids were hydrolized with sodium hydroxide (1 mol/L NaOH) for 12 hours. The hydrolized fatty acids were acidified with hydrochloric acid (1 mol/L HCl), and solvent was extracted, concentrated by evaporation, methylated with diazomethane, and cleaned up with a silica gel column. The absorption spectra were recorded on a Perkin–Elmer UV spectrophotometer with automatic scanner, using 10 mm fused silica cell, and registered on a Varian printer/recorder.

3. Results

In this section, three special slick experiments are discussed. On September 17, 1995, Doppler radar and ERS SAR data are analyzed together with in situ chemical samples. On September 18, 1995, the Doppler data and the corresponding chemical samples are discussed, while on September 21, 1995, only Doppler and ERS SAR data were available. The locations of these three experiments are shown in Figure 1. The section ends with some estimates of natural film coverage in the experimental region, using ERS 1/2 SAR imagery.

3.1. September 17, 1995

A slick experiment was performed on September 17, 1995, under moderate wind conditions (~3 m/s). The area investigated consisted of three distinct zones aligned in the offshore direction (Figure 4); a nearshore zone with small-scale roughness on the sea surface (zone 1), a smooth slick zone (zone 2), and a slightly rougher offshore zone (zone 3) on the other side of the slick. The RCS plot from the Doppler scatterometer (1750 UT, Figure 5a) shows a drop of 2.5 dB crossing from zone 1 into the slick zone 2 and an increase of 8 dB entering zone 3. The temperature and wind measurements obtained from the R/V *Håkon Mosby* indicated no atmospheric stability effects or changes in wind speed or direction when crossing the slick. The roughness difference (5.5 dB) between zone 1 and zone 3 (both nonslicked) is therefore interpreted to be caused by differences in biogenic content in these zones. Unfortunately, this interpretation cannot be tested, since no samples of the microlayer were obtained in zone 3 as a result of problems with the slick sampler. The backscatter at the edge of the plot in zone 1 (Figure 5a) is at the same level as that in the slick zone 2. This result may be due to parts of an east-west oriented slick visually observed to converge into the major north-south slick (Figure 4a).

With a ship speed of 2.3 m/s it took approximately 8 s to cross the slick. This finding implies a maximum slick width of 18.4 m, consistent with visual estimates of a 10-15 m wide (and ~10 km long) slick zone (Figure 4a). Abundant surfactant material was seen as scum and debris in the slick zone 2 (Figure 4). The corresponding current plot (Figure 5b) indicates a surface current (V_c) of 1.1 m/s in zone 1 and 0.9 m/s after crossing the slick (i.e., zone 3). The relative accuracy was estimated to be ±0.1 m/s, while the absolute accuracy was ±0.3 m/s (see the appendix for further details). A decrease in surface current of 0.2 m/s, over a distance of about 50 m, was observed when crossing the slick (Figure 5b). This implies the existence of a convergent current with a strain rate (convergence) of 4×10^{-3} s^{-1}, which is 1 order of magnitude larger than the Coriolis paramcter

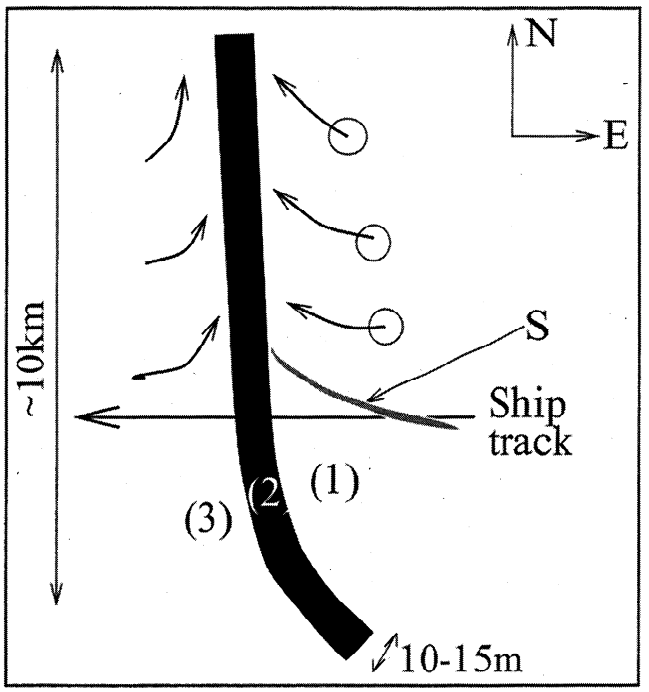

(a)

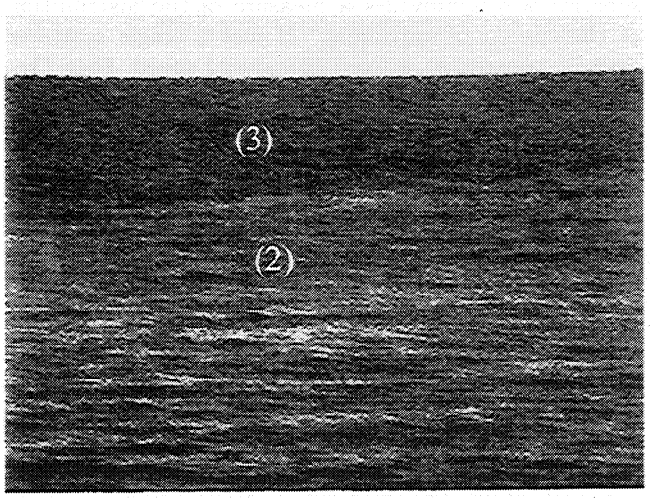

(b)

Figure 4. The slick study on September 17, 1995. (a) Cartoon and (b) photograph indicating (1) the rough zone, (2) the slick zone, and (3) the slightly rougher zone (zone 1 cannot be seen in the photograph). The slick was estimated to be about 10-15 m wide and ~10 km long. The current was stronger in the convergence zone (1) than in the slick zone (2). The circles indicate surface current drifters, and the long arrow gives the R/V *Håkon Mosby* ship track. Drawn in grey (marked S), crossing the ship track in zone 1, is an example of a smaller east-west oriented slick visually observed to converge into the major north-south slick.

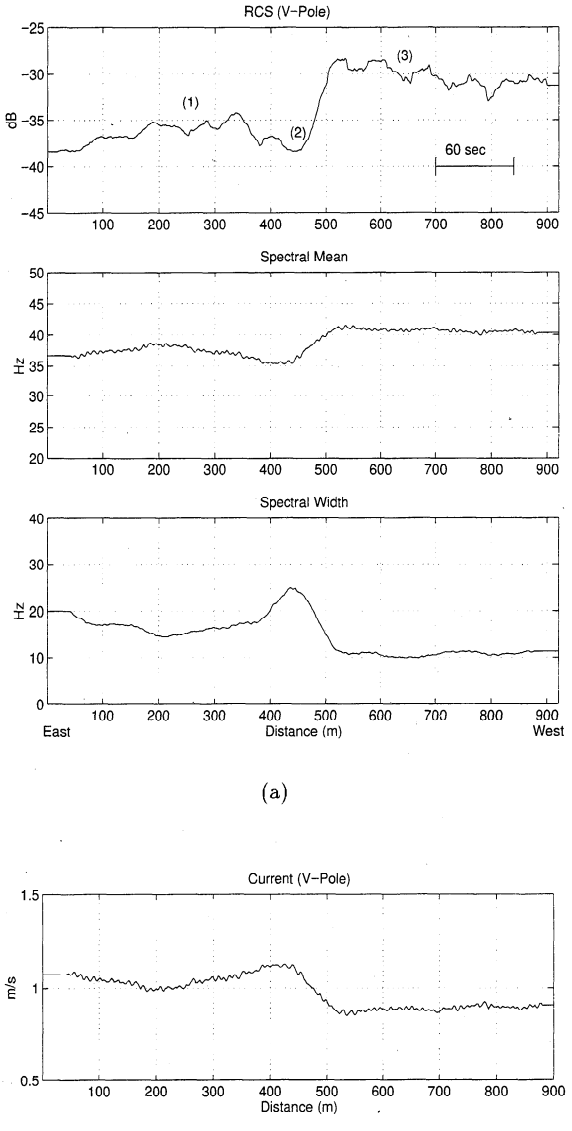

Figure 5. (a) Doppler radar results (radar cross section, spectral mean, and width) from September 17, 1995 (1750 UT) and (b) corresponding current plot. The different zones (see Figure 4) are indicated in the radar cross section (RCS) plot. The current velocity was obtained by converting the Doppler shift from the radar data to a horizontal velocity and subtracting the ship's speed, the Bragg wave phase speed, and the wind drift (estimated to be 3% of the wind speed). The entire plot may be shifted up or down 0.1 m/s as a result of uncertainties in all these factors as well as in the radar incidence angle.

($\sim 10^{-4}\ s^{-1}$), indicating a strong convergence. Figure 5b also indicates a slight increase in the current from zone 1 to zone 2. This increase is probably due to system noise effects associated with the low backscatter in the slick zone 2 (see section 2.2). The Doppler radar measurements are supported by observations of drifters deployed at the east side of the front (zone 1). The drifters were tracked by using a handheld GPS from a small rubber dinghy (~4 m long). One reading was obtained at the starting point of the drifters, and one was obtained at a later time. Care was taken not to disturb the drifters in manoeuvering the dinghy. The accuracy was estimated to be ±0.04 m/s over a distance of 7.5 km. The drifters were found to drift into the slick zone (northwestward direction) with a velocity of 0.70 m/s and then remain there (see Figure 4a).

The chemical analysis of the samples (zones 1 and 2, surface and bulk water) indicates that the surface microlayer was enriched both in fatty acids and in alkanes, in comparison with the corresponding bulk water samples (Table 1; the enrichment factor is the concentration of a substance in the surface microlayer sample divided by that measured in the corresponding bulk water sample). However, a clear difference was observed between zone 2 and zone 1 fatty acid and alkane concentrations. The slick sample (zone 2) was enriched 10 times in fatty acids in comparison with the bulk water, while the out-of-slick sample (zone 1) was enriched only about 1.5 times in comparison with the corresponding bulk water. The relative amounts of the different components of available fatty acids in inside and outside slick samples were similar in spite of these concentration differences. This finding indicates some connection between in- and out-of-slick material, consistent with the behavior of a converging current.

The ERS 2 SAR image from September 17, 1995 (1050 UT), was obtained 7 hours before sampling was done (Figure 6). This time difference was due to other commitments of the R/V *Håkon Mosby*. The in situ sampling was therefore performed on the basis of a visually observed slick. Later analysis showed that this slick cannot be seen in the SAR image; only areas near the coast have SAR-detected slicks (Figure 6). Evidence of film material extending offshore also is seen in the vicinity of the fjords. However, further offshore there is not enough film to cause damping in the SAR image. Accumulation of film material sufficient to be visually observed and measured by the Doppler radar must therefore have taken place during the 7 hours (with stable wind conditions of $\leq$5 m/s) between SAR imaging and in situ sampling.

3.2. September 18, 1995

On September 18 a thin slick oriented east–west was crossed (1120-1220 UT) perpendicularly (north to south) and diagonally (northwest to southeast) (Figures 7a and 7b, respectively). The slick was somewhat unevenly distributed, and the first crossing was wider than the second. A drop of 10.5 dB and 7 dB, respectively, can be seen in crossing into the slick zone. The most notable difference from the case on September 17 is that there is no major difference between the spectral mean and spectral width on either side of the slick, implying no difference in the current (see equation (A3) in the appendix). Therefore the slick must have been formed by a mechanism other than a converging current, or the converging currents had already dissipated and left the slick behind. Several surface drifters, deployed perpen-

Table 1. Summary of the COASTWATCH'95 Slick Experiment Results

		Film characteristics					SAR		Doppler	
Case	Date	ALK, μg/l	FA, μg/l	T, °C	SAL, ‰	WS, m/s	Damping, dB	Backscatter, dB	Damping, dB	Backscatter, dB
SM1(i)	Sep. 13	157.96	6.94	18.5*	35	2-3				
BU1(i)	Sep. 13	≤2.00	2.75	18.5*	35	2-3				
SM2(o)	Sep. 13			17.5*		2-3				
BU2(o)	Sep. 13			18.5*		2-3				
SM3(i)	Sep. 15			16.5*		9-10				
BU3(i)	Sep. 15			16.5*		9-10				
SM4(o)	Sep. 15	546.22	119.02	13.0*	30	9-10				
BU4(o)	Sep. 15	84.65	24.94	13.5*	35	9-10				
SM5(i)	Sep. 17	446.38	70.76		35	≤3			2.5	-38.0
BU5(i)	Sep. 17	130.22	8.38	14.3†	32	≤3				
SM6(o)	Sep. 17	176.79	4.60		33	≤3				-35.5
BU6(o)	Sep. 17	24.30	2.98	14.3†	35	≤3				
SM7(i)	Sep. 18	100.17	6.01		33	4			10.5	-33.0
BU7(i)	Sep. 18	119.20	10.57	14.4†	30	4				
SM8(o)	Sep. 18	24.83	15.30		34	4				-22.5
BU8(o)	Sep. 18	≤2.00	9.90	14.4†	32	4				
SM9(i)	Sep. 21					2-3	2.5	-13.2	8.0	-34.0
SM10(o)	Sep. 21					2-3		-10.7		-26.0
SM11(i)	Sep. 21					2-3	3.0	-13.5	12.5	-37.5
SM12(o)	Sep. 21					2-3		-10.5		-25.0

SM, surface microlayer; BU, bulk water samples taken at 20 cm depth; (i), in slick; (o), outside slick; FA, fatty acids (even-numbered C12-C18); T, temperature; ALK, alkanes (C18-C32); SAL, salinity; and WS, wind speed. Damping is the backscatter difference between inside and outside slick values (e.g., $dB_{SM6(o)}$-$dB_{SM5(i)}$).

* Measured from INTERFACE II (SM at 0-0.3 cm depth, BU at 20 cm depth).

† Measured from R/V *Håkon Mosby* (BU at 4 m depth).

dicular to the slick, measured an average drift speed of 0.50 m/s in a northwestward direction without any evidence of convergence toward the slick zone. The temperature measurements from the R/V *Håkon Mosby* indicate no atmospheric stability effects. The lower wind speed measured inside the slick area (~4 m/s) was 1 m/s lower than that measured outside the slick region (~5 m/s). There was no wind direction change. The wind speed difference cannot account for all the measured difference in backscatter (10.5 dB and 7 dB damp-

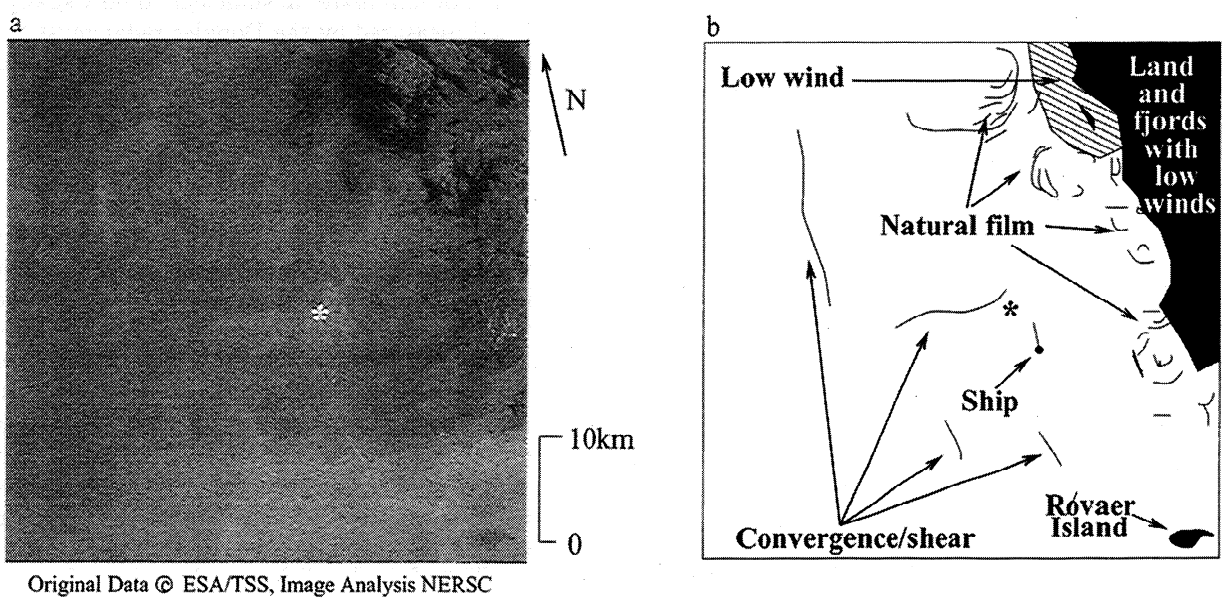

Figure 6. (a) A part of the ERS 2 SAR image taken on September 17, 1995 (1050 UT). In situ measurements were taken at the location of the asterisk, 7 hours after SAR imaging. Original data copyright ESA/TSS, image analysis NERSC. (b) An interpretation figure.

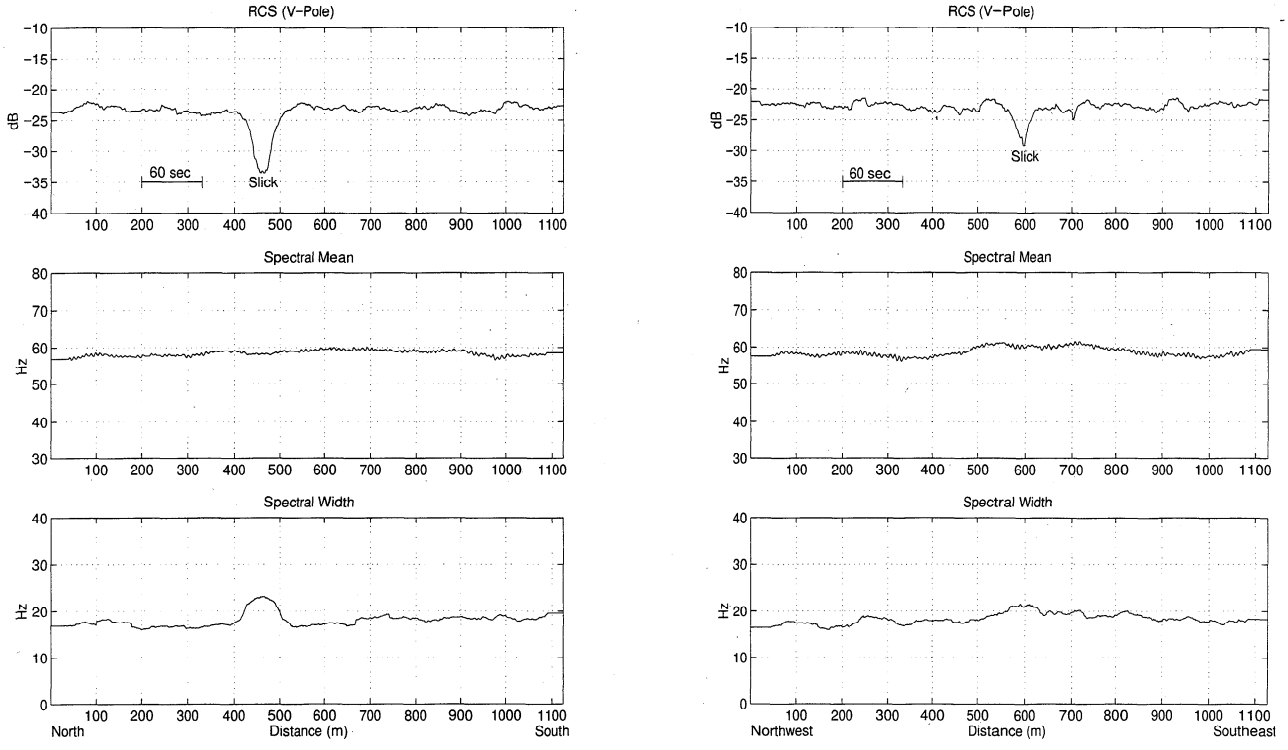

(a) (b)

Figure 7. Doppler radar results from September 18, 1995 (radar cross section, spectral mean, and width) crossing into the slick (a) perpendicularly and (b) diagonally.

ing). When the CMOD4 model [*Stoffelen and Anderson,* 1993] is used as an indication, a decrease from 5 m/s to 4 m/s wind will account for less than 2 dB difference in backscatter (for 45° incidence angle).

The chemical analysis revealed that concentrations and compositions of both fatty acids and alkanes were slightly different from the September 17 case (Table 1). However, the individual fatty acid compounds were the same as those reported earlier to dominate in sea surface film [*Larsson et al.,* 1974; *Daumas et al.,* 1976; *Kattner and Brockmann,* 1978; *Espedal et al.,* 1996]. The relative amounts of the different components of fatty acid were similar inside and outside the slick but distinct from the subsurface water. The last result is due to the different surface affinities of the compounds. The hydrocarbons (alkanes) present inside the slick were found at concentration levels lower than those for the September 17 case but still within the range of values reported by others for sea surface films [*Daumas et al.,* 1976; *Zsolnay,* 1977; *Espedal et al.,* 1996]. They were mostly straight and branched even-numbered alkanes, but some odd-numbered alkanes other than C_3 and C_5 appeared in the chromatograms. This finding suggests anthropogenic sources for up to 10% of the alkanes. Most of the branched hydrocarbons originate from bacteria [*Zsolnay,* 1977]. The composition of alkane organic matter was similar between surface microlayer and subsurface water but different between inside and outside slick samples. However, there were far fewer hydrocarbons than humic substances (long, coiled carbon-containing molecules) in the slick. Also, a higher proportion of humic substances was found inside than outside the slick. The estimates of surface film phenolic carbonaceous matter, measured as UV absorbance, suggested that these humic substances were mostly associated with particulate matter in the slick.

Unfortunately, no ERS SAR images were available for September 18, 1995. However, the existence of film material extending out from shore and fjords in the ERS 2 SAR image from the September 17 (Figure 6), and a fairly stable wind of less than 5 m/s between September 17 and 18, indicate that conditions were ideal for film accumulation.

3.3. September 21, 1995

A large slick area was crossed several times during the morning (1036-1100 UT) and early afternoon (1513-1542 UT) on September 21. In the first crossing (Figures 8 and 9) it can be seen that, similarly to the Doppler scatterometer results from September 18, there appears to be very little variation in the spectral mean (i.e., surface velocity; see equation (A3) in the appendix) in the slick free region. From the R/V *Håkon Mosby* a 0.5 m/s decrease in wind speed and a corresponding 30°-40° wind direction change were measured in crossing into the large slick zone. In a later crossing, finger-like extensions of the slick could clearly be seen (Figures 10 and 11). The minima in the spectral mean and maxima in spectral width shown in Figure 10 appear to be correlated with the low backscatter in the slicks. However, as we discussed in section 2.2, these

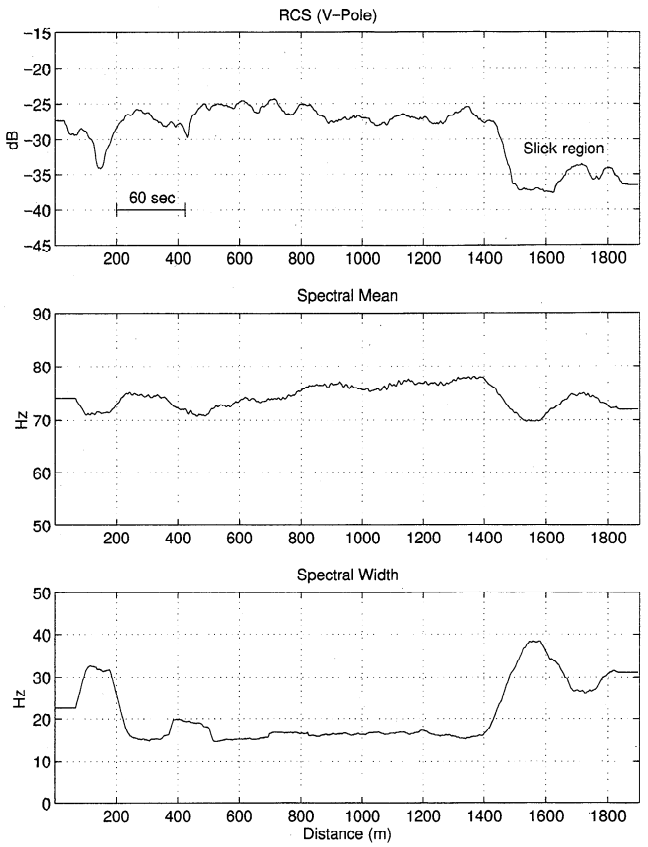

Figure 8. Doppler radar results (radar cross section, spectral mean, and width) for a crossing into a large continuous slick at 1051 UT on September 21, 1995.

correlations may be due to the effects of system noise associated with this low backscatter in the slick regions. Currents could therefore not be retrieved in the slick zones. Crossing the finger-like slicks took 400 s, with a ship speed of 3.9 m/s. This result indicates an approximate distance of 1.6 km. No in situ samples were collected during this interval, because another component of the COASTWATCH'95 experiment was in progress.

The ERS 1 SAR image from September 21, 1995, 2119 UT, clearly indicates that a slick was present in the investigated area (Figure 12). Hints of finger-like slick extensions can be seen near the sampling location. Their approximate size matches those found by the Doppler radar (~1-2 km). The 6 hours time lapse between the Doppler data and SAR imaging, and the prevailing low winds (~2-3 m/s), indicate that slicks can remain relatively unchanged on the ocean surface for several hours during calm weather conditions. The large slick area has disappeared totally in the ERS 2 SAR image of the region at the same time the next day. The wind speed increased from 2.5 m/s to 5-10 m/s during this period. This increase may imply a short lifetime for these slicks consistent with earlier suggestions by *Scott* [1986] that natural films disperse at winds above 7-8 m/s. However, *Demin et al.* [1985] found that film concentration actually increased for winds above 6 m/s but that their damping effect disappeared in the noise of wind-generated waves. Since no samples were obtained on September 22, 1995, this theory could not be tested here.

3.4. Quantification of Film Coverage

To investigate the dependence of observed films on wind speed and give an estimate of natural film distribution, 71 ERS 1/2 SAR images collected over the COASTWATCH'95 experiment region (in the period August-October 1995) were analyzed for slick signatures. It is by now a well-documented fact that several phenomena may dampen out the capillary and short gravity waves sensed by the radar (~7 cm waves for the ERS C band SAR) and cause dark areas, generally called slicks, in the SAR imagery [*Espedal,* 1998]. These phemomena include natural film, oil spills, produced water from oil platforms, grease ice, ship wakes, convergent current zones (e.g., along ocean fronts and eddies), rain cells, internal waves, threshold wind speed (≤2–3 m/s), wind sheltering by land or large platforms, and current wakes (created when ocean currents meet

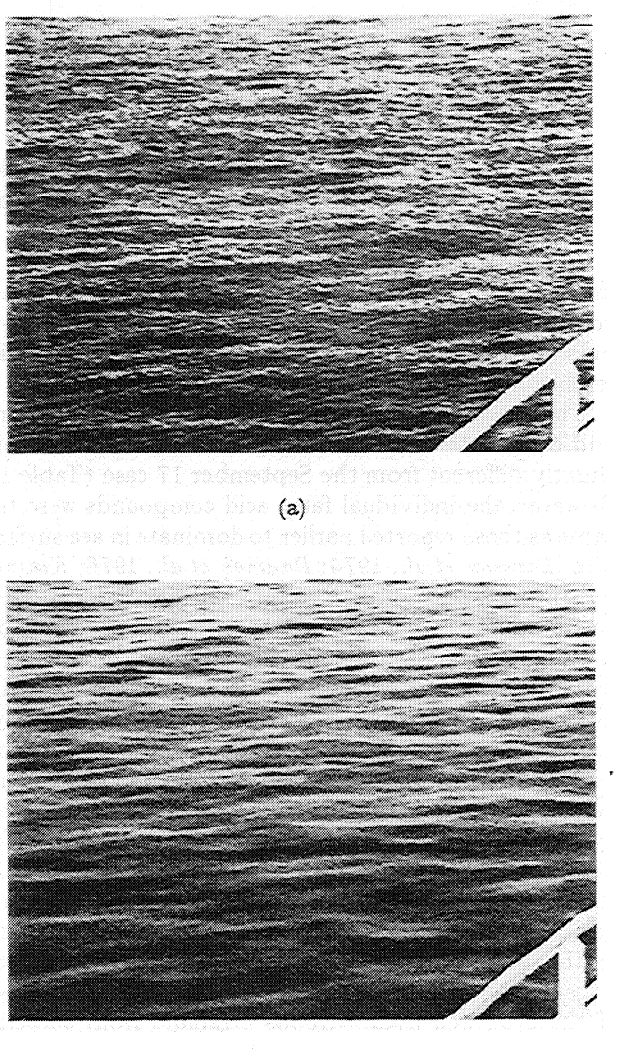

Figure 9. Contrast enhanced photos of (a) the slick free region, taken just prior to crossing into surfactant region, and (b) the slick.

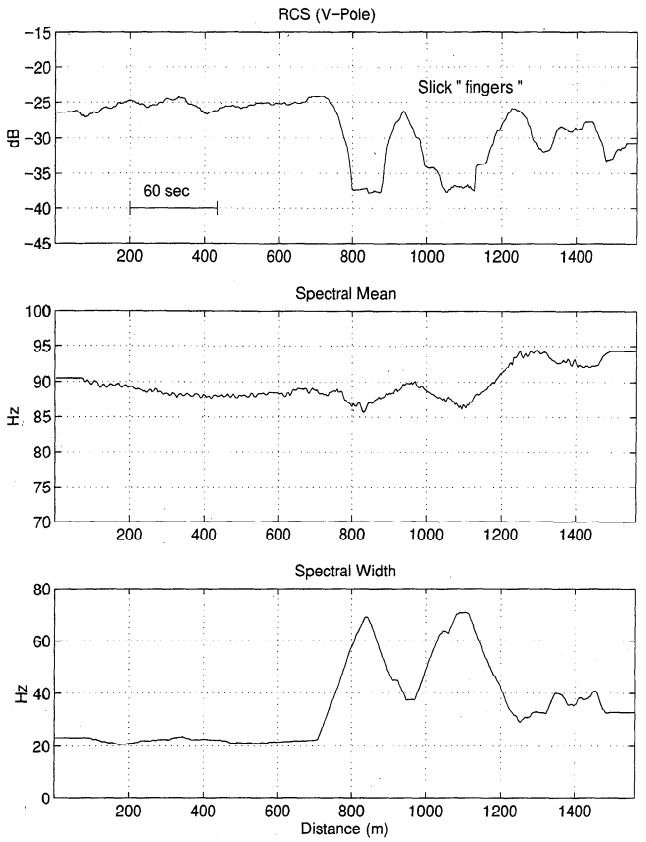

Figure 10. Doppler radar results (radar cross section, spectral mean, and width) for the crossing into finger-like extensions of slick material, at 1530 UT on September 21, 1995.

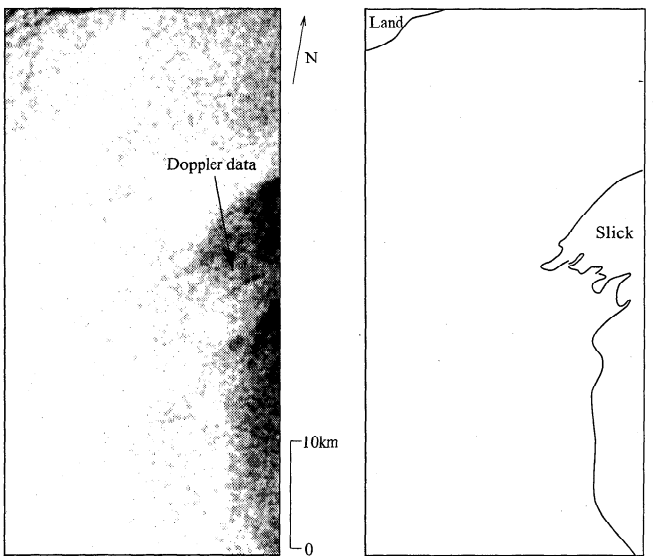

Original Data © ESA/TSS 1995

Figure 12. Part of the ERS 1 SAR image from September 21, 1995 (2119 UT). The location of the Doppler scatterometer data samples is indicated. Original data copyright ESA/TSS 1995. An interpretation figure, indicating the edge of the slick region, is shown to the right of the SAR image.

an obstacle such as a large platform). To discriminate between natural films and these similarly appearing features requires a direct analysis of the SAR image (shape, size, texture, gradients, and backscatter reduction of the slick; see box A in Figure 13) and a contextual analysis (meteorological data, currents, bathymetry, and platform and ship lane locations; box B in Figure 13). Some of the look-alikes (i.e., grease ice, convergent current zones, rain cells, and internal waves) are easily recognized on the basis of characteristic shapes and configurations and available weather information (i.e., air temperature and occurrence of precipitation). Produced water, wind sheltering, and current wakes can be ruled out on the basis of location (if oil platforms or land is nearby) and wind or current direction (if the slick is on the lee side of land or platforms). The main problems are caused by oil spills, low wind speed areas, or grease ice in the polar regions. Large oil spills are usually reported [*Johannessen et al.*, 1994] and can be ruled out. However, if smaller oil spills are classified as natural film, they will affect estimates for decibel values and damping by natural films. Since they are small, they will not cause large errors in estimates of natural film coverage. Low wind speed areas, however, can cover large areas; dark areas up to ~100 km long and ~50 km wide have been detected in SAR imagery [*Espedal*, 1998]. Such large homogeneous dark areas are classified as being caused by low winds, while large inhomogeneous slick features and systematic slick patterns, for example in eddies, are classified as being caused by natural film. In spite of the problems, satellite SAR could provide the first estimates of natural film coverage on a global scale. The methods for slick discrimination described above are in use at Tromsø Satellite Station (TSS) in their operational oil spill detection using ERS SAR imagery, performed in cooperation with the Norwegian Pollution Control Authority [*Wahl et al.*, 1993, 1994, 1996; *Espedal et al.*, 1995].

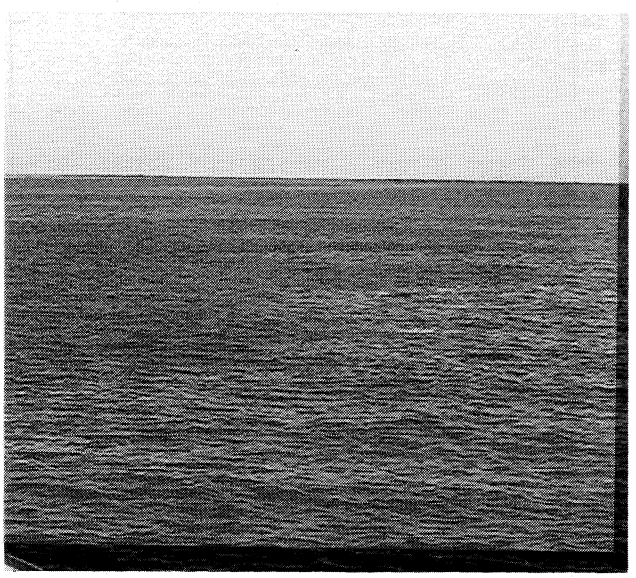

Figure 11. Photo of the slick "fingers" crossed during early afternoon on September 21, 1995.

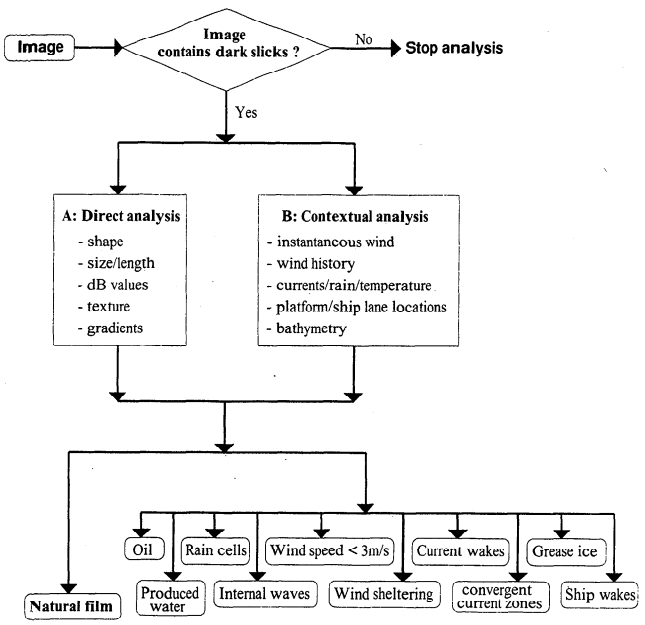

Figure 13. Outline of the main steps in a supervised natural film discrimination algorithm for SAR imagery.

Using the supervised slick discrimination algorithm in Figure 13, we obtained estimates for natural film coverage based on the 71 ERS 1/2 SAR images of the experiment region. Wind measurements were provided by the R/V *Håkon Mosby* or local weather maps, depending on which was closest in time and space to the investigated slicks. The plot in Figure 14 indicates that for increasing wind speeds the percentage of film coverage in the SAR scenes expectedly decreases. Many of the 71 investigated SAR scenes have the approximate same percent film coverage. The largest film coverages (up to 40%) are found for the lowest wind speeds, 2.5 m/s. For 5 to 10 m/s wind speed the natural film coverage has decreased below 5% in all cases. For 12.5 m/s and 15 m/s the coverage is below 1%. At such high wind speeds, natural film should not have been detected in the SAR imagery [*Demin et al.*, 1985; *Scott,* 1986; *Espedal,* 1998]. In these cases the wind speeds are believed to have been overestimated, since the slicks were found in or near fjords, where land sheltering may have a large effect on the local wind speed.

4. Discussion

Table 1 gives a summary of some of the results from the slick study in the COASTWATCH'95 experiment. The chemical analysis of the samples showed that trace metals were generally enriched in the surface microlayer, especially in the slicked areas. Trace metal enrichment is related to particulate matter present in the films, and possibly associated with humic substances (measured as UV absorbance). Humic substances were also enriched in the surface microlayer. Concentrations of free fatty acids indicate that these are raised inside slicks, but also in one of the samples where no slick was visually observed (Table 1, SM4(o)). This sample actually had the highest concentrations of fatty acids and alkanes mentioned in Table 1. The high wind speed (9-10 m/s) supports findings by *Demin et al.* [1985] that film is present (and its concentration may actually increase) at v≥6 m/s, but that its damping effect is hidden in the noise of wind-generated waves. Most fatty acids originated from marine organisms (plankton and macroalgae), since there are very few high molecular weight fatty acids available. The latter might have indicated higher plant material from terrestrial sources that could have been introduced from land (e.g., river runoff) via fjords into the coastal waters.

Using the temperature sensors on board the INTERFACE II slick sampler (see section 2.3), we measured the sea temperature between 0 and 0.3 cm depth for the surface microlayer and at about 20 cm for bulk water. The measurements from September 13 and 15, 1995 (Table 1) showed that the surface microlayer temperature was higher inside than outside the visually observed slicks (1°C and 3.5°C higher, respectively). On September 15 there was a full overcast, and the wind speed was 9-10 m/s. A patchy slick was observed despite the fact that the wind had remained at ≥7 m/s for several hours. This finding may indicate that the slick was caused by material other than natural film (e.g., oil). Unfortunately, no slick samples were obtained in this case. The slick/nonslick temperature difference of 0.3°C may be caused by reduced wave-induced mixing in the observed slick, causing more stratification in this region in comparison with the nonslicked area. Such a difference in stratification cannot be verified, since no temperature measurements were obtained at greater

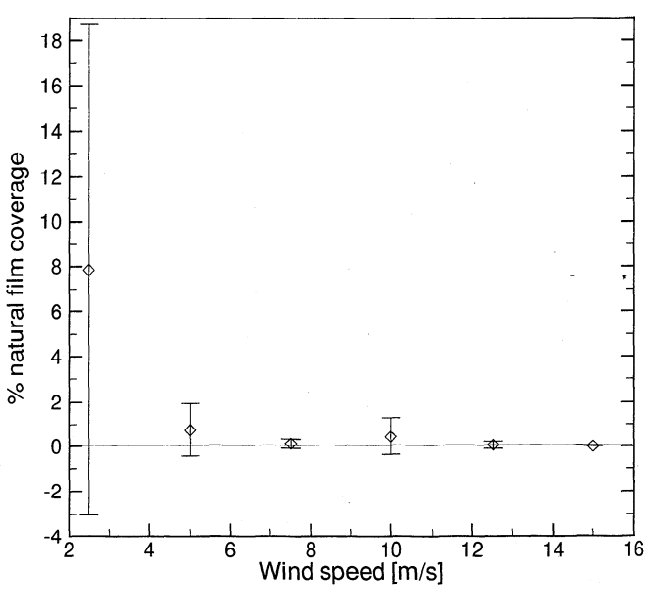

Figure 14. Plot of percent film coverage versus wind speed, based on natural films from 71 ERS 1/2 SAR scenes. The percent film coverage values are averaged at each wind speed, and the error bars indicate 1 standard deviation.

depths at these locations. However, on September 13 it was sunny, and the wind speed was only 2-3 m/s. The temperature difference (1°C) between in and out of the visually observed slick is most likely due to evaporative cooling of the slick-free surface. Temperature differences may also be caused by absorption of light energy by chemical species in films [*Alpers et al.*, 1982]. Such temperature differences caused by surface films are very important, since they affect stability and gas exchange rates. Further studies are therefore needed to improve the knowledge of the mechanisms responsible for these differences.

For the Doppler radar the damping values caused by the films described in Table 1 vary between 2.5 dB and 12.5 dB. These slicks were investigated during low to moderate winds ($\leq$4 m/s), and the different damping values therefore mainly depended on film composition and thickness variations. Low backscatter levels were observed to persist over distances ranging from 10 m to several hundred meters, depending on the width of the film. The overall RCS varied with wind speed and other environmental parameters (e.g., currents and slick presence) but stayed in the range between -20 and -40 dB (including cases not described in Table 1, where no SAR or slick sampling was available).

The damping in SAR backscatter caused by the films described in Table 1 was 2.5 dB and 3.0 dB, both investigated during low wind (2-3 m/s). No in situ sampling was performed, but the damped regions seemed to correspond well with damped areas found in the Doppler data.

The investigated natural films (including those not described in Table 1) generally gave higher damping values for Doppler radar than for SAR, when comparing 100 m resolution data. This result is probably due to a difference in noise floor and in Bragg wavelength (the wavelength observed by the radar), caused by the different incidence angles for the Doppler radar (45°) and the SAR (23°). The difference in radar frequencies (4.92 GHz for the Doppler radar and 5.3 GHz for the SAR) may also have a small effect here.

Backscatter values for natural film in the 71 ERS 1/2 SAR scenes investigated in this work varied between -6 dB and -26 dB (noise floor). The typical drop in backscatter caused by the natural films varied between 2 dB and 11 dB. The plot in Figure 15 indicates that increasing wind speeds expectedly lead to decreasing damping by natural film. The wide range of damping values, especially for low wind speeds, is probably due to varying film composition and thickness. Moreover, 27 SAR scenes were classified as showing no natural film (no damping). They all had a wind speed of 5 m/s or more.

In a comparison of the COASTWATCH'95 results (Table 1) with the slick sampling experiment carried out in Korsfjord southwest of Bergen, Norway (Table 2) [*Espedal et al.*, 1996], fewer and shorter C chain fatty acids were found during COASTWATCH'95. The short C chain fatty acid molecules are associated with marine organisms, while the longer ones come from terrestrial sources. Both experiments showed an approximate 1 order of magnitude increase of the concentration of fatty acids inside compared to outside films. For the Korsfjord case, backscatter decreases were found to vary between 6 dB and 17 dB, which is a slightly higher damping than that found in the COASTWATCH'95 cases (2–11 dB). This is probably due to differences in organic composition and concentration.

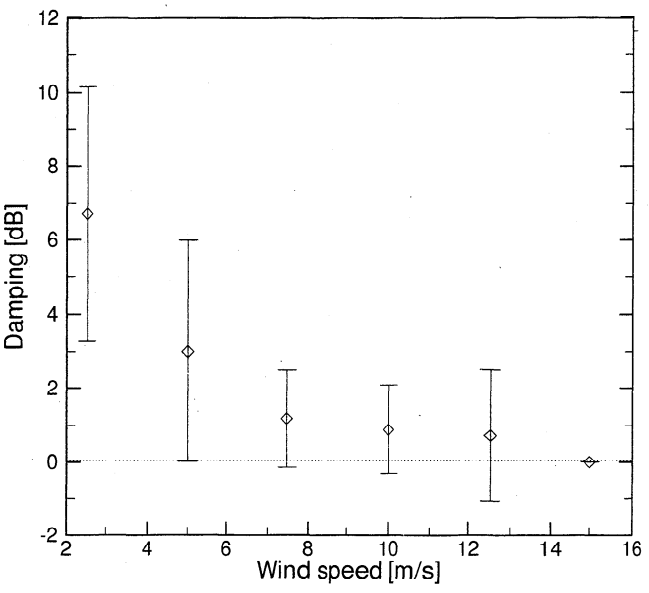

Figure 15. Plot of backscatter damping versus wind speed, based on natural films from 71 ERS 1/2 SAR scenes. The backscatter damping values are averaged at each wind speed, and the error bars indicate 1 standard deviation.

5. Conclusions

Using Doppler radar data and surface drifters, we were able to show that one geophysical process responsible for a verified natural film accumulation was convergence, while another verified film accumulation showed no clear convergence or shear. The damping by natural film was less in the SAR than in the Doppler data (both 100 m resolution). This result is probably due to a difference in noise floor and in the Bragg wavelength, caused by the different incidence angles and frequencies of the Doppler radar and the SAR.

A supervised natural film discrimination algorithm was used to obtain estimates of natural film coverage under different wind conditions. Up to 40% coverage was found for the lowest wind speeds (2.5 m/s), while at wind speeds of 5–10 m/s it had already decreased below 5% film coverage.

In comparison with an earlier fjord experiment [*Espedal et al.*, 1996] the investigated slicks during the COASTWATCH'95 experiment contained smaller fatty acid molecules, which indicated marine organisms as their source. In the fjord, terrestrial sources dominated. The slicks in the COASTWATCH'95 experiment with its lower concentration of fatty acids also resulted in slightly lower damping values (2–11 dB) in the ERS SAR imagery than in the fjord cases (6–17 dB).

Table 2. Summary of the Results from the Korsfjord Slick Experiment Performed on September 29, 1994

	Film characteristics			SAR	
Case	ALK, μg/l	FA, μg/l	WS, m/s	Damping, dB	Backscatter, dB
SMbuoy(i)	204	370	2.0		-8.5
BUbuoy(i)	27	351	2.0		
SM1(i)	431	1834	2.5	6.0	-14.9
BU1(i)	43	257	2.5		
SM1(o)	2	337	2.5		-8.9
BU1(o)	75	184	2.5		
SM2(i)	40	288	3.0	10.9	-19.7
BU2(i)	27	214	3.0		
SM2(o)	300	423	3.0		-8.8
BU2(o)	88	349	3.0		
SM3(i)	2	246	5.5	11.0	-18.7
BU3(i)	2	117	5.5		
SM4(i)	2	165	5.0	16.9	-24.6
BU4(i)	72	207	5.0		
SM4(o)	311	371	2.0		-7.7
BU4(o)	17	221	2.0		
SM5(i)	90	287	2.5	7.1	-14.8
BU5(i)	93	143	2.5		

SM, Surface microlayer; BU, bulk water samples taken at 50 cm depth; (i), in slick; (o), outside slick; FA, fatty acids; ALK, alkanes; and WS, wind speed. Damping is the backscatter difference between inside and outside slick values (e.g., $dB_{SM1(o)}$-$dB_{SM1(i)}$). For SM3(i) and SM5(i) the sample SM4(o) was used as a slick-free reference area. Summary data from *Espedal et al.*, [1996].

More studies are needed to extend the documentation of verified natural film simultaneously with satellite SAR coverage. On the basis of such increasing knowledge of natural film composition, as well as its behavior at different geographical locations and under different weather conditions, spaceborne SAR may eventually provide a very useful tool in mapping such films. This is important for satellite-based oil spill detection systems, since natural films and oil are look–alikes in SAR imagery. Natural films have also been seen to exert a significant effect on air–sea gas exchange. The extent, distribution, and variability of these films can therefore be important input parameters in global climate change studies.

Appendix: The Doppler Scatterometer

The C band (4.92 GHz) Doppler scatterometer utilized a single high-gain (22.5 dBi) pyramidal horn antenna with a mated ortho–mode transducer (OMT). The OMT allowed for transmission and reception of both horizontally and vertically polarized signals [*Dano and Kletzli*, 1996].

The CW scatterometer was calibrated by using several internal and external calibration procedures [*Ulaby et al.*, 1982]. The calibration results were used to determine the average RCS per unit area, as given by the relation

$$\bar{\sigma}^{\circ} = \left[\frac{Prx_{tgt}}{Prx_{cal}}\right] \cdot \left[\frac{\sigma_{cal}}{R_{cal}^4}\right] \cdot \left[\int \frac{g_n^2(\theta,\phi)}{R_{tgt}^4(\theta,\phi)} dA\right]^{-1} \quad \text{(A1)}$$

where Prx_{tgt} is the backscattered power received and Prx_{cal} is the power received from a calibration target of known RCS (σ) located a bore sight distance R_{cal} from the radar. The variable $g_n(\theta,\phi)$ is the antenna's normalized gain pattern, which, along with range to target, is relative to the radar aperture and integrated over the radar footprint after appropriate coordinate transformation. For experimental parameters used during COASTWATCH'95, equation (A1) can be written as

$$\bar{\sigma}^{\circ}(dB) = Prx_{tgt}(dB) - 5.98(dB) \quad \text{(A2)}$$

The spectral mean and corresponding currents were derived by using fast Fourier transforms (FFTs) on every 512 points (1 s) of band-pass-filtered (5-256 Hz) data. The spectral mean (or first moment) was found by taking the product of the spectral power density and the corresponding frequency. This quantity was summed over the entire spectrum and then divided by the total power to yield the spectral mean for a given FFT. This process was repeated for each FFT and then smoothed by taking a running 35 s average.

The surface currents were determined by using basic Doppler relations for an ocean environment [*Lee et al.*, 1995],

$$f_{d,obs} = [2 * sin(\theta)]/\lambda * [V_s + V_c + V_w + V_b] \quad \text{(A3)}$$

where $f_{d,obs}$ is the Doppler shift extracted from the radar data, λ is the wavelength (λ= 6.1 cm), and θ is the incidence angle (θ=45°). V_s is the radial ship speed, V_c is the component of the surface current velocity along the ship track direction, V_w is the component of the wind drift in the same direction (assumed to be 3% of the radial wind speed), and V_b is the phase speed of the associated Bragg wave. The Bragg wavenumber was found through the relation $K_b = 2 * K_r * \sin(\theta)$.

For an incidence angle θ=45° and a radar wavenumber of 103.0 R/m we determined a Bragg wavenumber of 145.67 R/m. Using the deep water approximation with appropriate constants (τ=0.074 N/m, g=9.81 m/s^2, ρ=1000 kg/m^3, K_b=145.67 R/m) yielded a Bragg wave phase speed of 0.28 m/s [*Crapper*, 1984].

When ship speed measurements with a nonstationary reference frame (the first measurement bin of the acoustic Doppler current profiler (ADCP) at 7–8 m depth) are used, absolute current measurements cannot be obtained. Thus the velocity of the current need not change sign at a given boundary to indicate a converging current (as would be expected in a fixed reference frame). An observed negative value of the current gradient, however, is indicative of a converging current.

On September 17 the spectral mean was 36.8 Hz prior to crossing the front and 41.4 Hz after crossing the front. The ship speed was 2.3 m/s (from ADCP measurements), and the wind was 2.3 m/s at 9° off the port bow of *Håkon Mosby*. The component of the wind drift velocity in the direction of the ship track is estimated to be 0.068 m/s. Equation (A3) thus yields a current of 1.06 m/s in the same direction as ship heading before crossing the front and 0.86 m/s after crossing. The plotted surface current in Figure 5b is the component along the ship heading (approximately east–west). The entire plot may be shifted up or down 0.1 m/s (relative accuracy) as a result of uncertainties in all these factors as well as in the radar incidence angle. To obtain absolute currents values for comparison with current drifters on September 17, ship speed was calculated by using GPS data of ship position at times t_1 and t_2. This method resulted in a ship speed V_s=2.3 m/s±0.3 m/s and thus current values similar to those calculated above. However, the absolute accuracy of the current values in this case is ±0.3 m/s.

Acknowledgments. The work of H.A.E. is funded by the Research Council of Norway. The COASTWATCH'95 experiment was a part of the Strategic Program for SAR remote sensing at NERSC, funded by the Research Council of Norway. Ship time was provided by the University of Bergen, and ERS 1/2 data were provided under the European Space Agency Program AO2.N108. The participation of E.D. and D.R.L. was made possible by funds provided by the Office of Naval Research under University Research Initiative grant N00014-92-J-1650 to the University of Michigan and by internal research funds provided by ERIM International, Inc.

References

Alpers, W., H.J.C. Blume, W.D. Garrett, and H. Hühnerfuss, The effect of monomolecular surface films on the microwave brightness temperature of the sea surface, *Int. J. Remote Sens., 3,* 457-474, 1982.

Alpers, W., V. Wismann, R. Theis, H. Hühnerfuss, N. Bartsch, J. Moreira, and J.D. Lyden, The damping of ocean surface waves by monomolecular sea slicks measured by airborne multi-frequency radars during the SAXON-FPN experiment, in *IGARSS '91, Remote Sensing: Global Monitoring for Earth Management, IEEE Publ. 91CH2971-0,* pp. 1987-1990, Inst. of Elec. and Electron. Eng., New York, 1991.

Asher, W., The sea surface microlayer and its effect on global air/sea gas transfer, in *The Sea Surface and Global Change,* edited by P. Liss and R. Duce, pp. 251-286, Cambridge Univ. Press, New York, 1997.

Crapper, G., *Introduction to Water Waves,* pp. 32-34, John Wiley, New York, 1984.

Dano, E., and D. Kletzli, Low cost CW scatterometers for field and laboratory use, in *Proceedings of the National Radar Conference,* IEEE Press, New York, 1996.

Daumas, R.A., P. Laborde, J.C. Marty, and A. Saliot, Influence of the sampling method on the chemical composition of water surface film, *Limnol. Oceanogr., 21,* 319-326, 1976.

Demin, B.T., S.A. Ermakov, N.Y. Pelinovsky, T.G. Talipova, and A.I. Sheremet'yeva, Study of the elastic properties of sea surface-active films, *Izv. Acad. Sci. USSR Atmos. Oceanic Phys., Engl. Transl., 21,* 312-316, 1985.

Duce, R., P. Liss, N. Blough, E. Bock, J. Hardy, K. Hunter, B. Jaehne, J. Plane, and A. Watson, The sea–surface microlayer and its potential role in global change, in *GESAMP working group 34, session 24, agenda item 7,* A&M Univ. Press, College Station, Tex., 1994.

Espedal, H., Oil spill and its look-alikes in ERS SAR imagery, in *Earth Observation and Remote Sensing,* Russ. Acad. of Sci., Harwood Academic Publishers, The Netherlands, in press, 1998.

Espedal, H.A., T. Hamre, T. Wahl, and S. Sandven, Oil spill detection using satellite based SAR: Pre-operational phase (A), *Tech. Rep. 102,* Nansen Environ. and Remote Sens. Cent., Bergen, Norway, 1995.

Espedal, H.A., O.M. Johannessen, and J.C. Knulst, Satellite detection of natural film on the ocean surface, *Geophys. Res. Lett., 23,* 3151-3154, 1996.

Frew, N., J.C. Goldman, M.R. Dennett, and A.S. Johnson, Impact of phytoplankton–generated surfactants on air–sea gas exchange, *J. Geophys. Res., 95,* 3337–3352, 1990.

Gershey, R., Characterization of seawater organic matter carried by bubble-generated aerosols, *Limnol. Oceanogr., 28,* 309-319, 1983.

Hara, T., E. Bock, and D.R. Lyzenga, In situ measurements of capillary-gravity wave spectra using a scanning laser slope gauge and microwave radars, *J. Geophys. Res., 99,* 12,593-12,602, 1994.

Harvey, G.W., Microlayer collection from the sea-surface: A new method and initial results, *Limnol. Oceanogr., 11,* 608-613, 1966.

Hühnerfuss, H., W. Walter, P. Lange, and W. Alpers, Attenuation of wind waves by monomolecular sea slicks by the Marangoni effect, *J. Geophys. Res., 92,* 3961-3963, 1987.

Hühnerfuss, H., A. Gericke, W. Alpers, R. Theis, V. Wismann, and P.A. Lange, Classification of sea slicks by multifrequency radar techniques; New chemical insights and their geophysical implications, *J. Geophys. Res., 99,* 9835-9845, 1994.

Jessup, A., W. Melville, and W. Keller, Breaking waves affecting microwave backscatter, 1, Detection and verification, *J. Geophys. Res., 96,* 20,547-20,559, 1991.

Johannessen, J.A., G. Digranes, H.A. Espedal, O.M. Johannessen, P. Samuel, D. Browne, and P. Vachon, SAR Ocean Feature Catalogue, Spec. Publ. *ESA SP-1174,* Eur. Space Res. and Technol. Cent., Noordwijk, The Netherlands, 1994.

Johannessen, O.M., et al., COASTWATCH-95: ERS 1/2 SAR applications of mesoscale upper ocean and atmospheric boundary layer processes off the coast of Norway, *Proc. Int. Geosci. Remote Sens. Symp. '96, 11,* 1158-1161, 1996.

Kattner, G.C., and U.H. Brockmann, Fatty-acid composition of dissolved and particulate matter in surface films, *Mar. Chem., 6,* 233-241, 1978.

Keller, W., and W. Plant, Cross sections and modulation

transfer functions at L and Ku bands measured during the Tower Ocean Wave and Radar Dependence Experiment, *J. Geophys. Res., 95,* 16,277-16,289, 1990.

Knulst, J.C., Interfaces in aquatic ecosystems: Implications for transport and impact of anthropogenic compounds, doctoral dissertation, Lund Univ., Lund, Sweden, 1996.

Larsson, K., G. Odham, and A. Sødergren, On lipid surface films on the sea, I, A simple method for sampling and studies of composition, *Mar. Chem., 2,* 49-57, 1974.

Lee, P., J. Barter, K. Beach, C. Hindman, B. Lake, H. Rungaldier, J. Shelton, A. Williams, R. Yee, and H. Yuen, X band microwave backscattering from ocean waves, *J. Geophys. Res., 100,* 2591-2611, 1995.

Lucassen-Reynders, E., and J. Lucassen, Properties of capillary waves, *Adv. Colloid Interface Sci., 2,* 347-395, 1969.

Scott, J.C., Surface films in oceanography, *Workshop Rep. C-11-86,* pp. 19-34, Office of Naval Research London, 1986.

Stoffelen, A., and D.L.T. Anderson, ERS 1 scatterometer data and characteristics and wind retrieval skills, in *Proceeding of First ERS 1 Symposium, Eur. Space Agency Spec. Publ., ESA SP-359,* 1993.

Ulaby, F.T., R.K. Moore, and A.K. Fung, *Microwave Remote Sensing: Active and Passive,* vol. II, pp. 746-779, Artech House, Norwood, Mass., 1982.

Wahl, T., T. Anderssen, and Å. Skøelv, Oil spill detection using satellite based SAR: Phase 1B, completion report, Norw. Def. Res. Estab., Kjeller, 1993.

Wahl, T., T. Anderssen, and Å. Skøelv, Oil spill detection using satellite based SAR: Pilot operation phase, *final report,* Norw. Def. Res. Estab., Kjeller, 1994.

Wahl, T., et al., Radar satellites: A new tool for pollution monitoring in coastal waters, *Coastal Manage., 24,* 61–71, 1996.

Walker, D., D.R. Lyzenga, E. Ericson, and D. Lund, Radar backscatter and surface roughness measurements for stationary breaking waves, *Proc. R. Soc. London A, 452,* 1953-1984, 1996.

Wismann, V., Radar signatures of mineral oil spills measured by an airborne multi-frequency radar and the ERS 1 SAR, *IGARSS '93, IEEE Publ. 93CH3294-6,* pp. 940–942, Inst. of Elec. and Electron. Eng., New York, 1993.

Zsolnay, A., Inventory of nonvolatile fatty acids and hydrocarbons in the oceans, *Mar. Chem., 5,* 467- 475, 1977.

E. Dano, Department of Naval Architecture and Marine Engineering, University of Michigan, Ann Arbor, MI 48109. (e-mail: ebd@engin.umich.cdu)

H. A. Espedal and O. M. Johannessen, Nansen Environmental and Remote Sensing Center, Edvard Griegsvei 3A, 5037 Solheimsviken, Norway.
(e-mail: Heidi.Espedal@nrsc.no; Ola.Johannessen@nrsc.no)

J. A. Johannessen, European Space Research and Technology Centre, P.O. Box 299, 2200 AG Noordwijk, The Netherlands. (e-mail: jjohanne@estert.jw.estec.esa.nl)

J. C. Knulst, Swedish Environmental Research Institute (IVL), Aneboda, S-36030 Lammhult, Sweden.
(e-mail: johan.knulst@ivl.se)

D. R. Lyzenga, Environmental Research Institute of Michigan, Ann Arbor, MI 48109.
(e-mail: lyzenga@erim.org)

(Received February 24, 1997; revised March 26, 1998; accepted May 13, 1998.)